GEOTECHNICAL ASPECTS OF SEPT. 5, 2012 M7.6 SAMARA, COSTA RICA EARTHQUAKE

Version 1.0

January 30, 2013

Prepared by

Kyle Rollins and Kevin Franke
Brigham Young University

Ronaldo Luna and Nicholas Rocco
Missouri University of Science and Technology

Daniel Avila
Utah Department of Transportation

Alvaro Climent M.
Instituto Costarricense de Electricidad (ICE)

Table of Contents

1. Seismological Background

The Samara (Nicoya) Costa Rica earthquake occurred at 8:42 am local time (14:42 UTC) on September 5, 2012. The epicenter of the 7.6 M_w earthquake was located approximately 10 km off the shore of Samara at 9.777º and -85.569º and at a depth of 14.2 km as shown in Fig. 1.1 according to the Laboratory of Engineering Seismology (LIS) at the Univ. of Costa Rica. However, the USGS located the epicenter below the Nicoya Peninsula (10.099°N 85.308°W at a depth of 35 km to 40 km. Costa Rica lies above a convergent plate boundary where the Cocos plate is subducting beneath the Caribbean Plate at a rate of 77 mm/yr (USGS, 2012). The earthquake occurred as a result of thrust faulting on the plate interface. A plot of epicenter and hypocenter locations versus depth for the main event (USGS location) and subsequent aftershocks is provided in Fig. 1.2 (LIS, 2012a) and clearly defines the thrust fault geometry. This plot also shows that much of the energy release was occurring directly under the Nicoya peninsula. A subsequent analysis of the fault rupture history indicates that rupture started near the surface (epicenter located by LIS) and propagated down the dip of the fault to the northeast. (see animation, LIS (2012c,d). This plot also shows that much of the energy release was concentrated at 30 to 40 km below ground. Apparently, the LIS epicenter is located near where the fault rupture initiated while the USGS epicenter is located near the center of the energy release. As shown in Fig. 1.3, the maximum slip displacement was approximately 2.5 m.

The USGS provides the following summary of the earthquake history in the region:

> "Over the past 40 years, the region within 250 km of the September 5th earthquake has experienced approximately 30 earthquakes with M 6 or greater; two of these were larger than M 7, and neither caused documented fatalities. The first was a M 7.2 in August of 1978, 9 km to the north-northeast of the September 5th 2012 event; the second had a magnitude of M 7.3, and struck a region just over 50 km to the east-southeast in March 1990. The earthquake of October 5, 1950, M 7.8, occurred in the general area of the September 5th 2012 earthquake, although the hypocenter of the earlier earthquake is not known to high precision"

Table 1.1 provides a table of measured maximum accelerations along with station name and Mercalli Scale classifications for the 32 recording stations from the Engineering Seismology lab(LIS). Stations are ranked from highest to lowest acceleration. Additional details regarding each station, including available geological information and the ground motions they recorded, are available from LIS at http://www.lis.ucr.ac.cr/index.php?id=Estaciones. The peak ground accelerations shown in Table 2.1 are plotted geographically in a color coded fashion in Fig. 1.1. The highest recorded motion was 1.38 g at the library in Nosara which was about 15 km from the fault rupture. Peak acceleration are above 0.34 g in the Nicoya Peninsula. The peak accelerations general decrease as one moves northeast from the rupture surface. However, a review of the distribution of accelerations in Fig. 1.1 indicates that there is a concentration of unexpectedly high peak accelerations (yellow points) relative to the lower adjacent station accelerations at similar distances (blue and green points). This concentration of higher accelerations levels is thought to be related to soil amplification or topographic effects in this region.

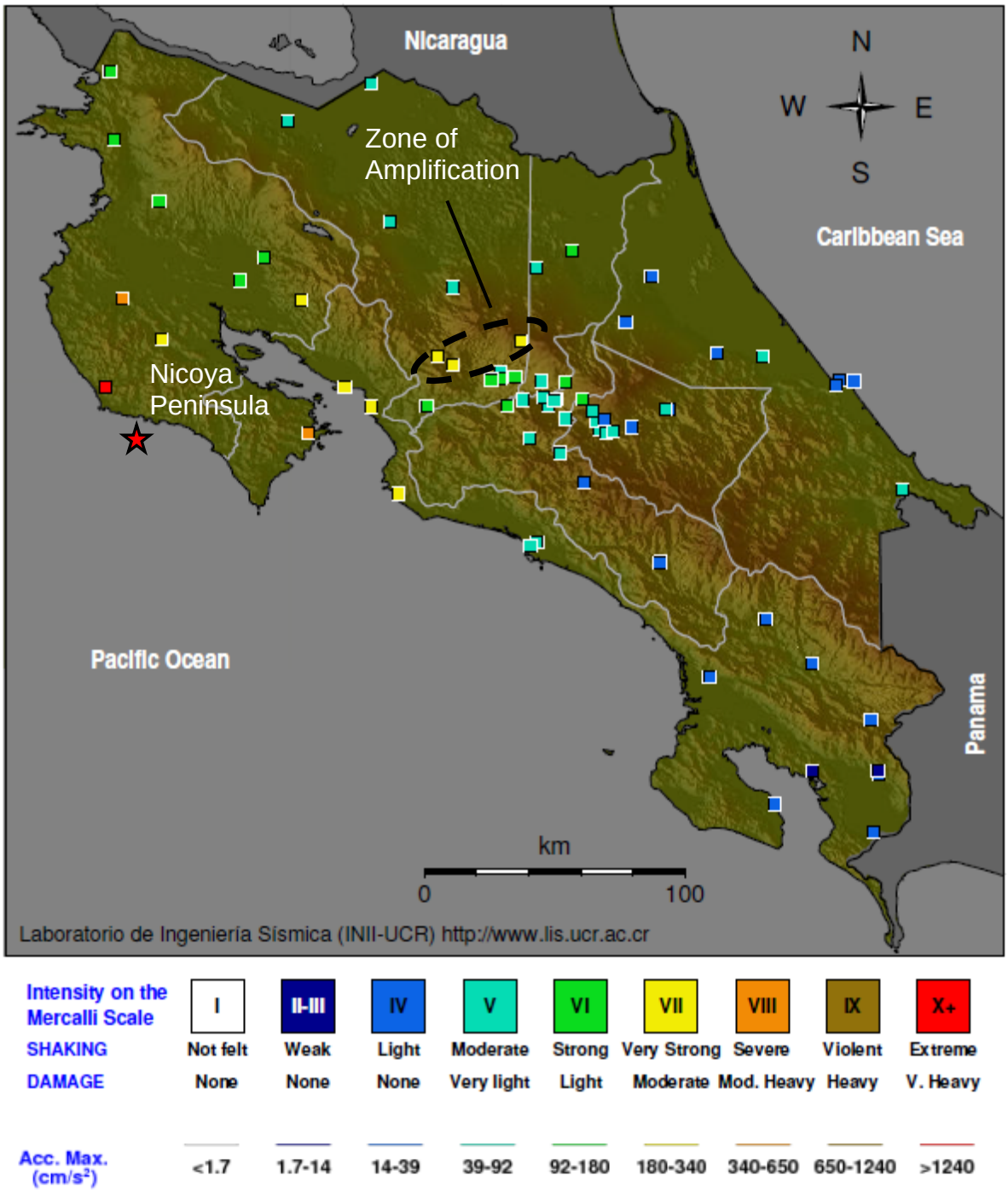

Fig. 1.1 – Location of epicenter and peak ground accelerations measured by the seismic network operated by the Engineering Seismology Laboratory (LIS) at the University of Costa Rica. The recordings are color coded according to the acceleration level and Mercalli scale categories shown at the base of the map (LIS, 2012a).

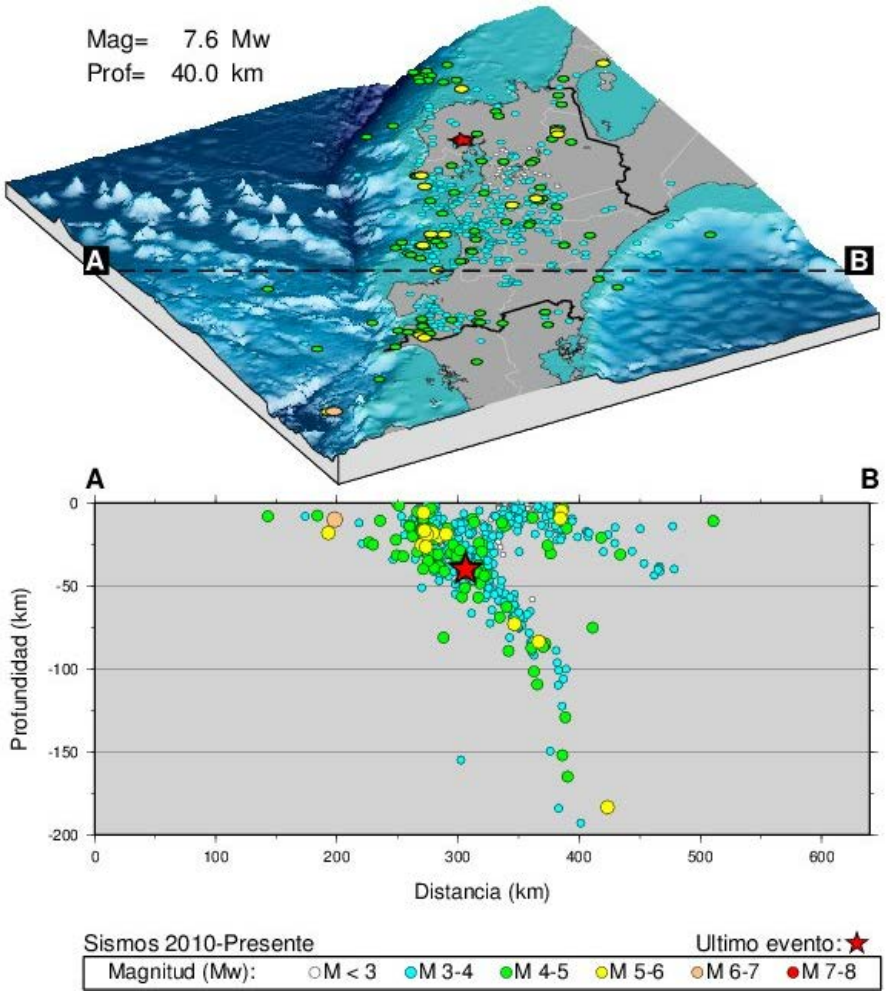

Fig. 1.2 – Plan and profile view of epicenters and hypocenters since 2010 and the main shock highlighted with a red star. This pattern delineates the boundaries of the rupture zone and the geometry of the thrust fault (LIS, 2012a)

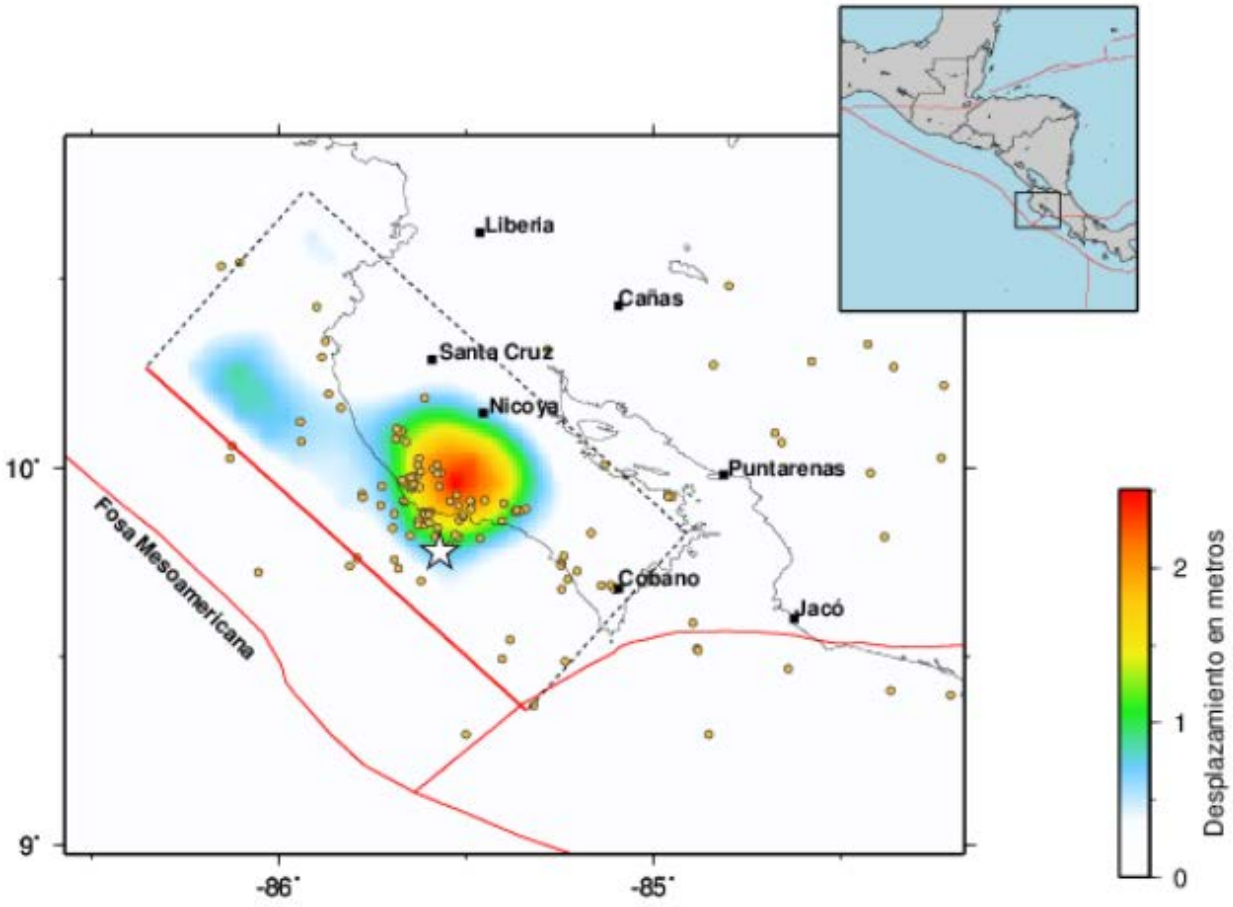

Se muestran los rasgos tectónicos más importantes de la región como las fallas activas (trazas de color rojo) que delimitan los bordes de las placas tectónicas. El modelo de falla obtenido en este estudio se superpone sobre le mapa lo cual permite tener una mejor idea de los lugares donde el desplazamiento fue particularmente grande. La línea punteada del rectangulo de la falla es la proyeccion de esta a profundidad. La parte superior de la falla seria la linea continua roja.

Fig. 1.3 Plan view drawing showing color contours of the fault rupture displacements obtained by researchers at the Laboratory of Engineering Seismology (LIS) at the University of Costa Rica (LIS, 2012c)

Table 1.1 Summary of maximum acceleration and Mercalli intensity at each recording station (LIS, 2012a)

Station	Acceleration	Mercalli Intensity	Place (location)
Estación	Aceleración (cm/s^2)	Intensidad (IMM)	Lugar
GNSR	1376.40	X+	Biblioteca de Nosara
GSTC	563.02	VIII	Sede UCR, Santa Cruz
PPQR	428.79	VIII	Cruz Roja, Paquera
AFRA	284.06	VII	Sede UCR, Fraijanes
ASRM	262.92	VII	Sede UCR, San Ramón
GNYA	239.67	VII	INS, Nicoya
PCDA	218.97	VII	INCOP, Caldera
PPUN	211.63	VII	Sede UCR, Puntarenas
GJTS	205.87	VII	Las Juntas, Abangares
APMR	204.09	VII	Biblioteca, Palmares
PJAC	181.49	VII	Cruz Roja, Jacó
GCNS	145.63	VI	Biblioteca, Cañas
AALA	137.69	VI	INS, Alajuela
AORT	135.91	VI	Cruz Roja, Orotina
GSTR	132.68	VI	Parque Santa Rosa
GTGA	132.13	VI	Ingenio Taboga, Cañas
AFBR	122.33	VI	Est. Fabio Baudrit, Alajuela
HPVJ	120.35	VI	Municipalidad Sarapiqui
CTRH	117.81	VI	Hosp Chacon Paut, Tres Ríos
GLIB	117.10	VI	Sede UCR, Liberia
SCCH	117.06	VI	Ebais Ciudad Colón
RGAR	116.80	VI	Recope Barranca
GLCR	109.93	VI	Cruz Roja, La Cruz
HCPD	100.14	VI	San Miguel, Sto. Domingo
ASCS	91.69	V	Biblioteca, Ciudad Quesada
SIAC	88.56	V	Municipalidad, Acosta
STRN	85.18	V	Teatro Nacional
CPAR	84.39	V	Sede UCR, Paraíso
SSBN	82.73	V	ICODER, La Sabana
AUPA	82.47	V	Municipalidad, Upala
SCGH	82.42	V	Hosp. Calderón Guardia
AMTR	80.99	V	Asoc.Des. Monterrey, San Carlos
SHTH	70.25	V	Clínica de Hatillo
ACLS	60.11	V	Cruz Roja, Los Chiles
SFRA	60.07	V	Frailes
CCDN	58.67	V	Ciudad de los Niños, Agua Caliente
RALT	54.06	V	Recope El Alto
SGTS	53.75	V	Escuela Guatuso, Patarrá
SJUD	53.08	V	Saint Jude School, Santa Ana
HVRG	51.78	V	Cruz Roja, La Virgen
SMSO	50.98	V	Museo del Oro, San Jose
CCRT	46.72	V	Biblioteca,Cartago
CHLM	46.22	V	Holcim, Cartago
HHDA	46.20	V	Cruz Roja, Heredia
PQSH	44.91	V	Hospital Quepos
CTUH	44.26	V	Hosp William Allen, Turrialba
ACAR	44.05	V	Presa Carrillo, Alajuela
PQUE	42.89	V	Bomberos, Quepos
LBTN	41.32	V	Cruz Roja, Batan
LTAL	39.69	V	Colegio, Talamanca
CSRH	37.04	IV	San Rafael, Oreamuno
CTBA	36.91	IV	Sede UCR, Turrialba
PBNA	36.27	IV	Municipalidad, Buenos Aires
CCHI	32.99	IV	Cachi
SSMD	31.76	IV	Casa de Pan, Santa María de Dota
LCAR	29.69	IV	Cruz Roja, Cariari
SISD	27.46	IV	INS, San Isidro de El General
LGPI	27.17	IV	Sede UCR, Guápiles
SISH	27.02	IV	Rg Brunca,S Isidro
LMOI	26.82	IV	Pto. Moín, Limón
PPTG	25.93	IV	Cruz Roja, Potrero Grande
RMOI	25.68	IV	Recope Moín
LLIH	25.55	IV	Hospital Limón
POSA	22.59	IV	Municipalidad, Puerto Cortés
PLRL	20.86	IV	Oficina Acueducto Laurel, Corredores
PJMN	20.24	IV	Colegio, Puerto Jiménez
LSQR	18.20	IV	INS, Siquirres
PSVT	17.64	IV	Bomberos San Vito
PCNH	15.67	IV	Hospital C. Neily
PCNL	13.50	II-III	Bomberos, Ciudad Neily
PGOL	4.84	II-III	Sede UCR, Golfito

Fig. 1.4 provides a plot of measured peak acceleration versus hypocentral distance for 25 of the ground motions listed in Table 1.1. The data generally follow a linear trend on a log-log plot; however, as noted previously, there are a number of recording stations at distances between 100 and 130 km where the peak ground acceleration is two to three times higher (0.2 to 0.3g) than accelerations (0.1 to 0.15g) for other recording stations at comparable distances. These are the recording station mentioned previously in Fig. 1.1 and correspond to stations in San Ramon, Palmares and Fraijanes, Costa Rica. The GEER team worked to visit some of these recording stations and measure shear wave velocity profiles to determine if this could help explain the higher accelerations. These measurements are reported subsequently in section 5 of this report.

Based on the measured accelerations from the recording stations, seismologists from LIS developed contours of peak acceleration/Mercalli Intensity values throughout Costa Rica for the main earthquake event. These contours show a lobe of higher accelerations within the yellow contour extending into the center of the country while surrounding acceleration zones are lower (green contour band) (LIS, 2012b)

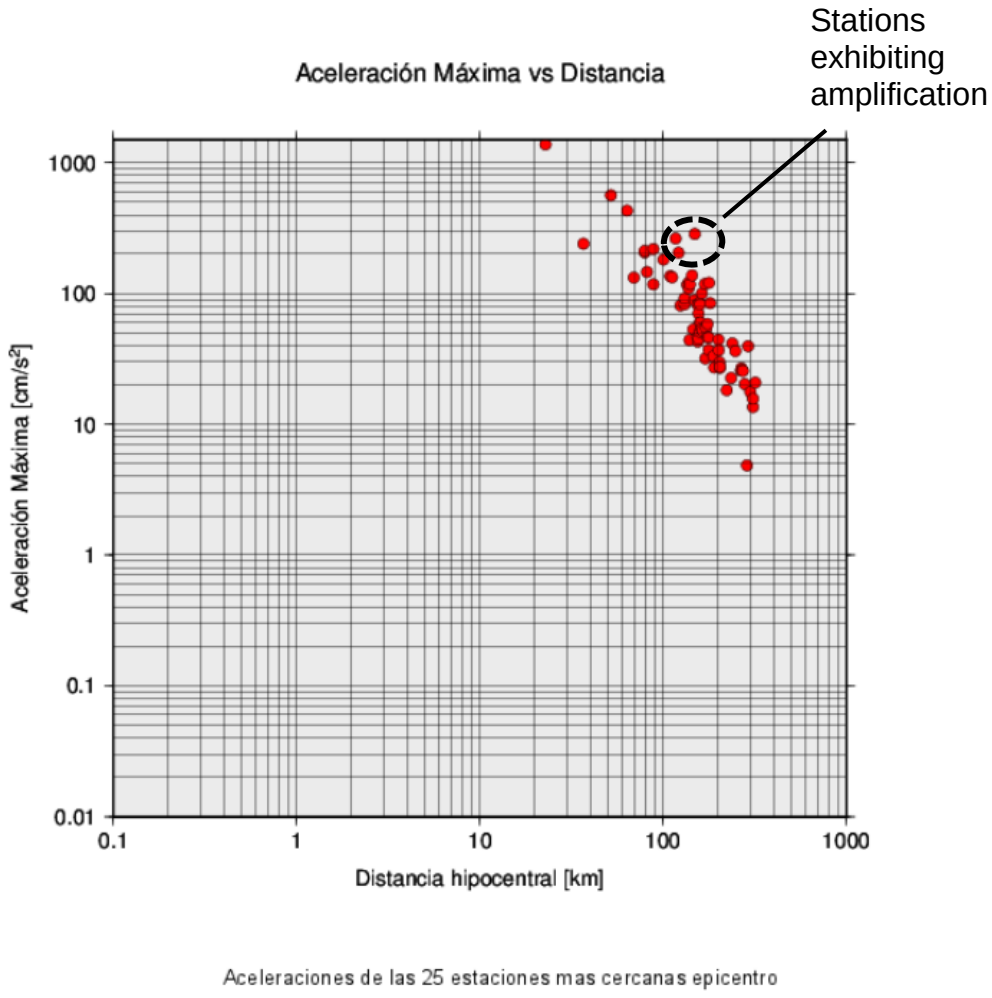

Fig. 1.4 Peak Ground motion versus hypocentral distance for 25 recording stations. (LIS, 2012a)

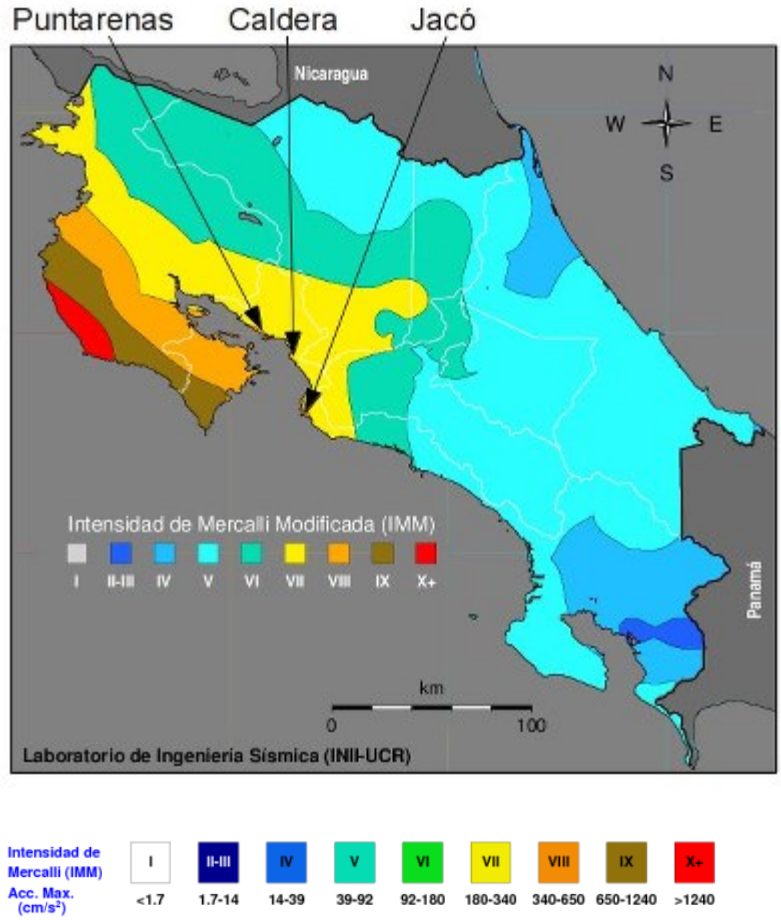

Fig. 1.5 Contours of peak ground acceleration/Mercalli Intensity throughout Costa Rica based on the recorded ground motions (LIS, 2012b). Note lobe of higher acceleration within the yellow contour band.

2. Liquefaction

In contrast to the M7.5 1991 Limon, Costa Rica earthquake the M7.6 2012 Samara, Costa Rica earthquake produced relatively little liquefaction induced damage to infrastructure. During the 1991 earthquake the epicenter was located in the eastern side of the country as shown in Fig. 2.1; whereas the 2012 earthquake had an epicenter located off the western coast of the country. As indicated by the geologic map of Costa Rica (Dutch, 2012), the surficial geology of the eastern side of Costa Rica is dominated by recent sedimentary deposits which consist of loose saturated sands near the coastline which are liquefiable. In addition, both the major east-west highway from the capitol city of San Jose to the port city of Limon on the Caribbean coast, as well as the major highway paralleling the coast, traverse these liquefiable zones. As a result, in the 1971 earthquake 13 bridges were significantly damaged or collapsed as a result of liquefaction induced lateral spreading (Youd et al, 1992). In addition, 30% of the paved roadway surfaces were broken up along the coastal highway. These roadways and bridges were critical to the regional economy and this led to the loss of several million dollars in revenues.

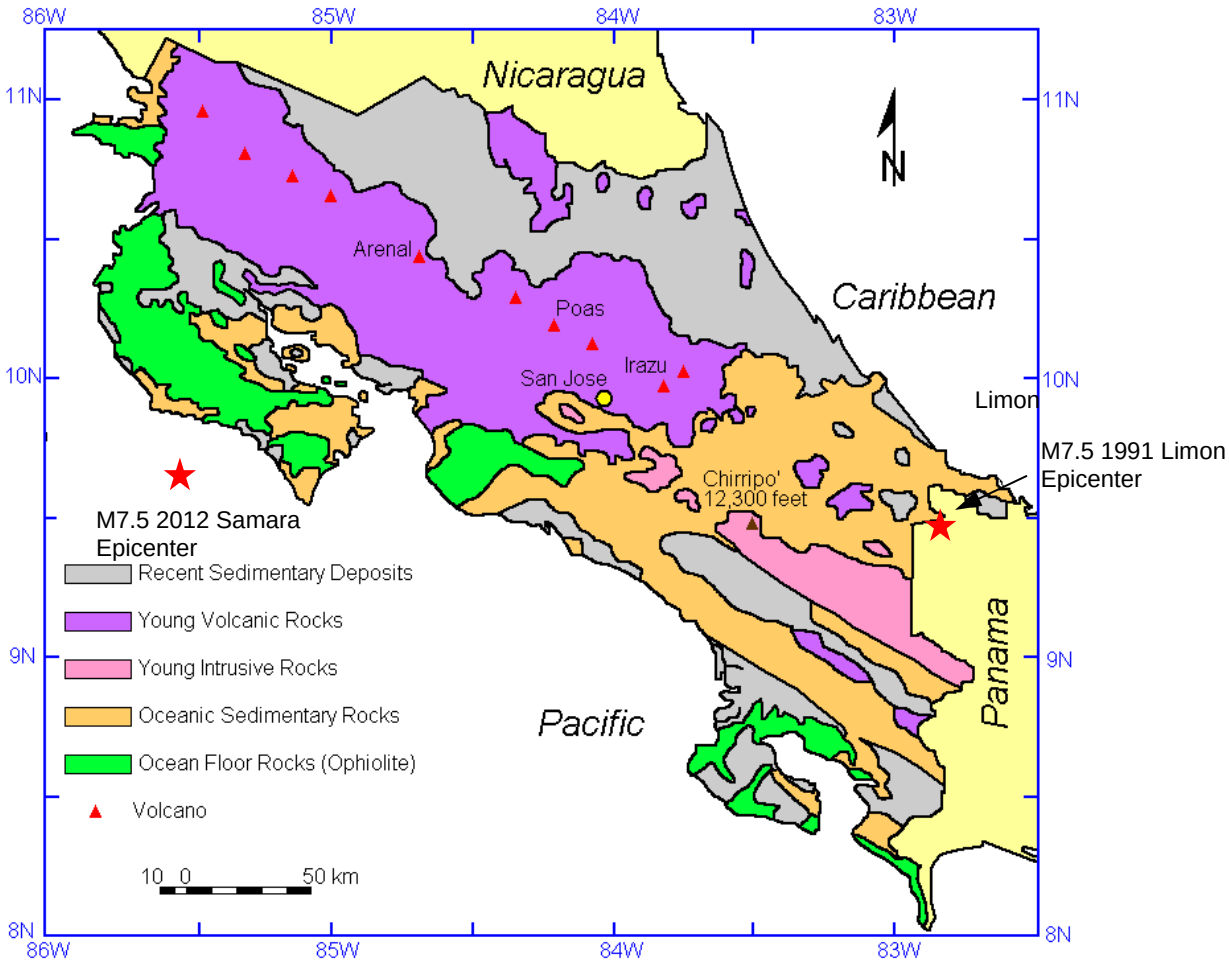

Fig. 2.1 - Geology map of Costa Rica (modified from Dutch 2012) with locations of epicenters from M7.5 1991 Limon Earthquake and M7.6 2012 Samara Earthquake

In contrast, the surficial geology of the western side of Costa Rica, including the Nicoya peninsula, is dominated by sedimentary rocks and recent sedimentary deposits are quite rare (see Fig. 2.1). These sedimentary deposits are typically associated with river alluvium and beaches. Although a limited number of bridges cross over rivers in the region, there is little infrastructure traversing the beaches. These circumstances may help explain the relatively lower level of liquefaction induced damage in the 2012 earthquake relative to the 1991 event. These results also point out the value and importance of geologically based liquefaction hazard mapping.

Despite these geological conditions, liquefaction was clearly observed in susceptible deposits during the earthquake. Fig. 2.2 shows the locations were liquefaction was reported in the earthquake. Liquefaction features were reported at seven beaches along the coast of the Nicoya peninsula and in Puntarenas. Peak ground accelerations near the western coast line may have ranged from 0.4g to over 1.0g, but were typically around 0.2 g in the vicinity of Puntarenas. Photographs of the liquefaction features at several of the beaches are shown in Fig. 2.3. In one case at Playa Ostional a large sand boil can be recognized, but at most locations the cracking patterns are indicative of liquefaction induced settlement and lateral spread movements. In some cases, the offsets in the cracks were wider than 30 cm and the crack were as deep as 1.5 m. As noted in the photo credits, these photos were all obtained from internet searches because these features were obscured by tides and waves at these beach locations by the time the GEER team visited these sites.

Fig. 2.2 - Google earth map of Costa Rica showing location where liquefaction features were observed during the 2012 Samara earthquake.

(a)

(b)

(c)

(d)

(e)

Fig. 2.3 - Liquefaction features at beaches in the 2012 Samara Earthquake. (a) man standing in lateral spreading cracks Playa Pochote (Alvarez, 2012) (b) lateral spreading cracks at Playa Garza (Reuters, 2012a) (c) sand blow at Playa Ostional, (d) Cracks at Playa Tivives (Edodes, 2012) (e) Cracks, up to 5 ft deep, at Ostional beach (Cotza Rica, 2012)

2.1 Liquefaction of Shallow Foundations – Capitanía de Puerto, Puntarenas

Liquefaction damage was observed at a site in Puntarenas, a relatively thin barrier peninsula within the Gulf of Nicoya. This city is one of the largest along the Pacific coast and several other port facilities are located nearby. Port services are available within this city and on the north side of the peninsula there is a small office for port security and fisheries. The Capitanía is a port of entry office in charge of security and shipments. This building is a relatively small structure built on concrete pedestals or stilts supported on shallow foundations. The structure was recently renovated (6 months previously) and a handicapped ramp was installed. The entire structure rotated as a monolith during the earthquake when the foundation soils liquefied. The foundations punched through the liquefied ground at different rates to produce the tilting and failure of some of the reinforced 12-inch square concrete stilts (see Fig. 2.4). It is estimated that the building sank about 50 to 75 cm. The building was supported on nine (9) 30cm square concrete stilts. Each column foundation had a clear crater developed around the footing. The center stilt developed a crater of about 2.6 meters wide and 0.6 m deep.

Fig. 2.4 - Capitanía Port Office in Puntarenas (9.978153° N 84.840758° W)

Fig. 2.5 – Foundations Punching through liquefied ground (a) exterior column, north side; (b) interior column, left behind a 60cm crater.

Fig. 2.6 – Structure tilted toward he west side (a) west side bottomed out at the top of the water tank; (b) new handicapped ramp detached from building front porch.

After the field reconnaissance of the property and surrounding ground an MASW geophysical survey was carried out about 20 feet away from the structure damaged due to liquefaction. Fig. 2.7 shows the location of the survey and the shear wave velocity (V_s) profile. The upper 5 meters varied between 100 and 150m/s, several cracks were also observed at the ground surface, probable indication of oscillation of fill soils on top of liquefied ground. From 5 to 15 meter depth the V_s increased linearly to 200m/s and then more firm ground reached a V_s of up to 400m/s. Clearly, the ground near the surface was quite loose and unstable with numerous surface cracks.

Damaged water and sewer utilities that served the Capitanía building office.

Location of the MASW geophysical survey on the north side of structure.

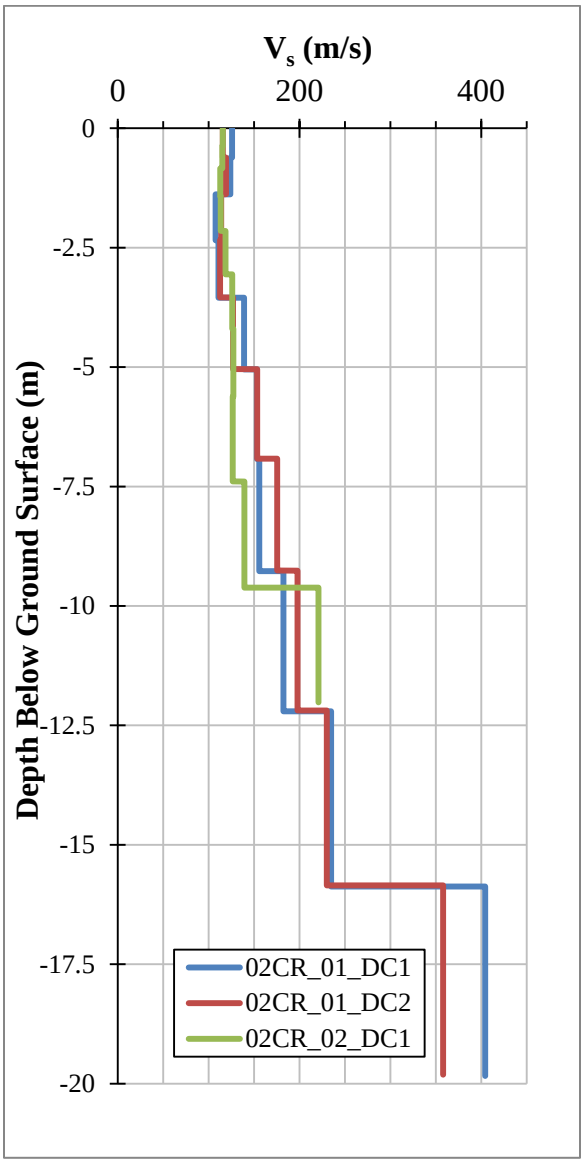

Fig. 2.7 - MASW Shear Wave Velocity (V_s) Profile near the Capitanía Office Building, which was subjected to liquefaction failure. (Lat. 9°58'41.35"N / Long. 84°50'26.73"W)

2.2 Tambor Beach Hotel

A 200+ room hotel at Tamblor beach experienced significant damage during the earthquake. Although the hotel remained open to accommodate some guests after the earthquake, the damage was sufficient that the hotel stopped accepting guests and had go close several months for repairs to the hotel buildings and swimming pool areas. The GEER team drove to this hotel, shown in Fig. 2.8, but was not permitted to enter the grounds. Given the proximity of the hotel to the sandy beach area and the liquefaction observed at other similar beach locations along the coast of the Nicoya peninsula, it is likely that liquefaction played a role in the damage to the hotel.

Fig. 2.8 Hotel at Tambor Beach which sustained significant damage and was closed for several months to undertake repairs to the hotel and swimming pool areas. Given proximity of sandy soils, liquefaction likely played a role in the damage.

3. Performance of Ports and Pier

3.1 Puerto Caldera

The Puerto Caldera on the Atlantic coast of Costa Rica, shown in Fig. 3.1, is the largest port facility in the country and handles over 3 million metric tons of cargo per year. Cargo typical includes about 75% grains and 25% minerals. The port also serves a couple cruise liners and has a small passenger arrival terminal. The port was constructed on fill material in 1981 by the Costa Rican government and is operated as a private concession. The wharf is composed of steel sheetpile walls and has 490 m of waterfront with depths of 7.5, 10, and 11 m. An additional length of wharf with a depth of 13 m is currently under construction.

A seismograph station (PDCA) operated by the University of Costa Rica Laboratory of Engineering Seismology (LIS) is located within a few hundred meters of the port facilities, as shown in Fig. 3.1, and recorded a peak ground acceleration of 0.22 g during the earthquake.

Fig. 3.1 - Puerto Caldera, Puntarenas relative to location of UCR LIS seismograph station PDCA which recorded a peak ground acceleration of 0.22g (9.91055° N 84.7167° W) Courtesy of Google Earth

Damage to the port was relatively minor and cargo operations continued after the earthquake without significant problems. A continuous concrete beam was originally constructed parallel to the wharf to support a track mounted crane. That crane was subsequently replaced by a mobile crane unit which was under routine maintenance at the time of the quake and was therefore lightly loaded. Settlement of the surrounding soil relative to the continuous beam were generally less than 8 mm but in some local areas settlement troughs were as great as 100 mm as shown in Fig. 3.2.

(a) **(b)**

Fig. 3.2 - (a) Earthquake induced settlement in local zones adjacent to the longitudinal beam running parallel to the wharf (9.91197° N 84.72112° W). (b) Settlement was approximately 100 mm (4 inches).

At the west and east ends of the port, rectangular zones appeared to heave upwards relative to the surrounding ground suggesting that some underground structure was made buoyant during the earthquake as shown in Fig. 3.3.

(a) **(b)**

Fig. 3.3 - Apparent heave of rectangular area on the (a) west (9.91170° N 84.72194° W) and (b) east (9.91246° N 84.71811° W) ends of the port.

As indicated by the photo in Fig. 3.4, the wharf did not show any signs of lateral spreading or outward deformation. Differential settlement of the floor slab in the cruise passenger waiting area was sufficient to cause cracks in the tile floor in two directions. At the time of our visit the damaged tile had been removed, the slab leveled and tile was being replaced. In an adjacent warehouse facility the columns were all supported by piles which did not settle. Most of the columns had been protected from impact damage by forming a circular concrete column around the steel column. In most instances, the concrete floor slab remained flush with the bases of these concrete columns. However, in several cases, the base slab settled between 70 mm and 100 mm (2.5 to 4 inches) relative to column base as shown in photograph in Fig. 3.4. Settlement of this magnitude in saturated fill material suggests liquefaction; however, the floor slabs were able to accommodate this settlement without cracking and there was no indication of sand boils at the port.

(a) **(b)**

Fig. 3.4 - (a) Concrete cylinders protecting pile-supported columns in warehouse adjacent to wharf and (b) earthquake induced settlement of the ground around the column relative to the pile-supported column. (9.91192° N 84.72003° W

3.2 Puerto de Moin

The other major port in Costa Rica is located on the Caribbean coast which was over 270 km from the rupture surface. Peak ground accelerations in this vicinity were on the order of 0.027g (stations RMOI and LMOI, LIS network). There were no reports of any damage to this port facility for these low acceleration levels.

Puerto Puntarenas

As shown in Fig. 3.5 and Fig. 3.6, the pile-supported pier at Puntarenas extends approximately 550 m offshore and was constructed in 2002 in collaboration with the Taiwanese government. The port is a routine stop for several cruise liners such as Celebrity and Holland America. The first 350 m section of the pier is supported by steel pipe sections which are approximately 150 mm (6 inches) in diameter. Based on a commemorative sculpture near the pier, the 150 mm piles

appear to have been drilled into place using expendable augers approximately 0.6 m in diameter and 1.0 m in length. The main pier (200 m length) used to moor the cruise ship appears to be supported by steel piles or caissons approximately 0.6 m in diameter. Two additional dolphins were located beyond the pier itself.

Damage to the pier was visible during our visit, but appeared to be relatively minor and primarily limited to the pile-supported section of the pier. The pier has remained operational since the earthquake, though sections of damaged railing were blocked off with orange cones for safety concerns. A lateral offset of about 76 mm (3 inches) was measured between the pile- and caisson-supported sections of the pier (Figs. 3.7 and 3.8). Damage to the 100mm-diameter steel guardrail of the pier, particularly on the west side, was visible in various locations throughout the rotated portion. Several portions of the railing were pulled apart approximately 76 mm (3 inches) as shown in Fig. 3.9, presumably due to extension on the west side of the pier. No evidence of buckling in the railing was visible on the east side of the pier. The connections between the guardrail posts and the pier were significantly damaged throughout much of the pile-supported section of the pier (Fig. 3.10). From our observations, it appeared that many of the railing posts had been previously welded, perhaps from a need to temporarily remove the railing for some type of pier maintenance. In nearly every location where damage was observed in the connection between the guardrail and the pier, damage to or failure of the weld was observed (Fig. 3.11). A utility pipe, presumably water, was observed on the west side of the deck of the pier. The pipe appeared to have sustained some cracking in a few locations along the pile-supported section of the pier (Fig. 3.12). At this point, security personnel approached the reconnaissance team requesting that no more photos be taken of the pier. However, the security personnel allowed the team to continue its investigation and to note its observations. A 38-meter portion of the pile-supported section appeared to have rotated slightly resulting in a 25 mm (1 inch) gap in the deck slab on the west side of the pier and crumbling/spalling of the deck slab on the east side of the pier due to compression and pounding. Further evidence of pounding between deck slabs was observed approximately 105 meters from the head of the pier on the pile-supported section.

Inspection was performed in the vicinity of the beach at the head of the pier. No evidence of liquefaction or lateral spread was observed. However, it is possible that liquefaction and/or lateral spread in the submerged soil contributed to the observed rotation of the pier section.

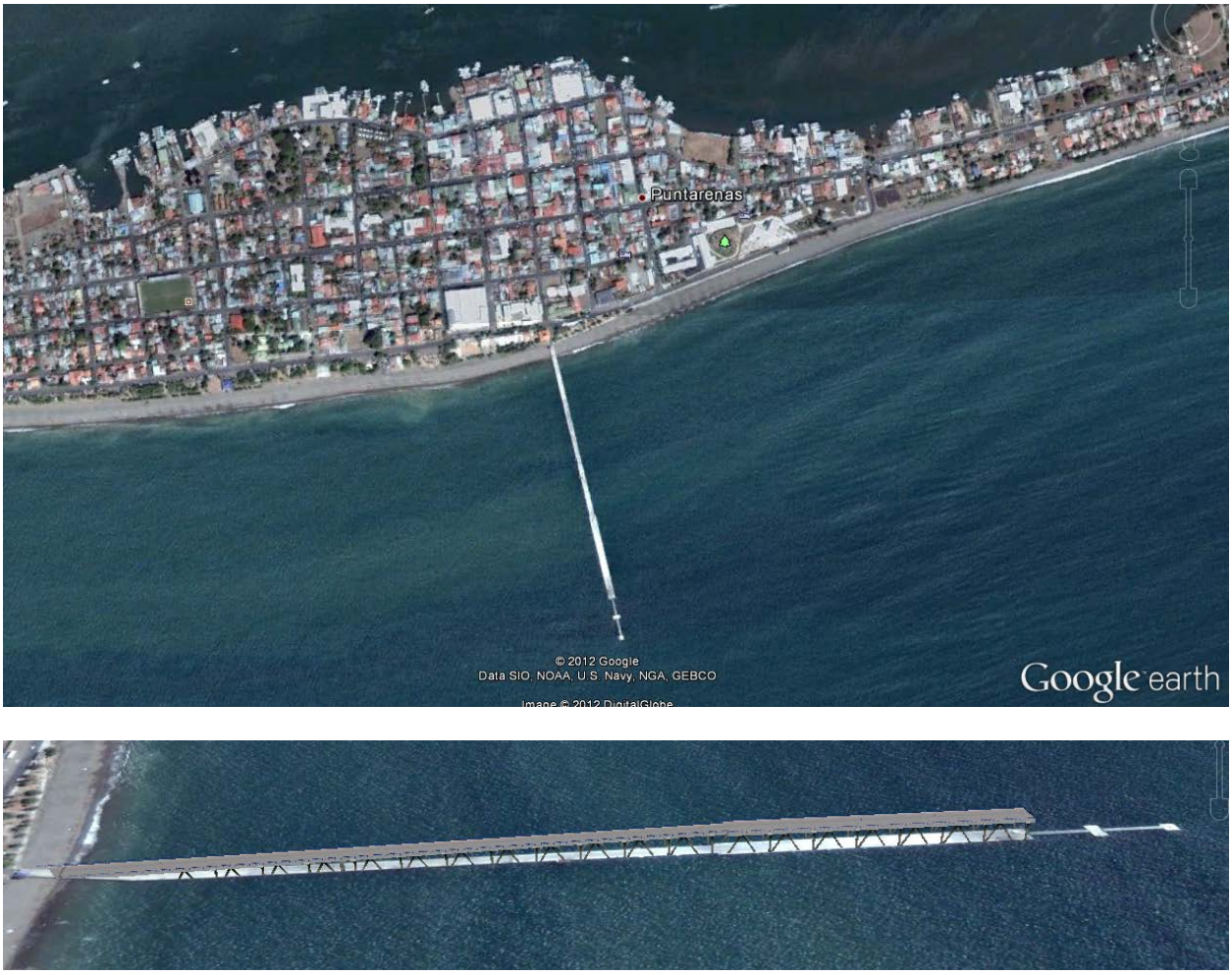

Fig. 3.5 - Aerial view and 3-dimensional representation of the Puerto Puntarenas (courtesy of Google Earth ™)

Fig. 3.6 - 3-dimensional replication of the Puerto Puntarenas (courtesy of Google Earth ™)

Fig. 3.7 - Lateral offset between the pile- and caisson-supported sections of the pier (9.97177° N 84.83068° W).

Fig. 3.8 - Lateral offset between pile- and caisson-supported sections of the pier (facing south).

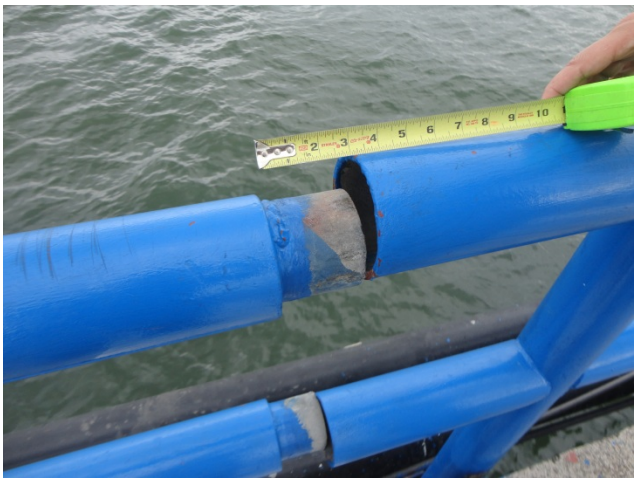

Fig. 3.9 - Sections of the steel guardrail that had pulled apart during the earthquake (9.97205° N 84.83078° W).

Fig. 3.10 - Damaged connection between a guardrail post and the pier (9.97213° N 84.83079° W).

Fig. 3.11 - Sheared weld on a damaged guardrail post. Similar damage was observed on nearly every post (9.97214° N 84.83070° W).

Fig. 3.12 - Damaged water pipe adjacent to pier (9.97190° N 84.83075° W).

3.3 Pier at Doubletree Hotel, Puntarenas

The pier at the Doubletree Hotel in Puntarenas is a pile-supported structure which extends approximately 150 m towards the ocean as shown in Fig. 3.13.

Fig. 3.13 - (a) Plan (Google Earth) and (b) elevation views of the damaged pier at Doubletree hotel in Puntarenas

The reinforced concrete deck is 8 ft wide and consists of two T-beams 6 inch wide and 24 inches deep. The deck is supported by two 14 inch square pre-stressed concrete piles which are spaced 25 ft on centers longitudinally and 6 ft on centers in the transverse direction. The piles are battered in the transverse direction at about 15º from vertical or 4V:1H to provide increased lateral stability. Aluminum cross-bracing was added between the piles to provide some additional longitudinal stability. The piles are connected to the deck by two 21 inch square capitals connected by a reinforced concrete cross-beam. The piles extend 10 to 25 ft above the surface of the beach sand.

Based on nearby seismograph stations, the pier was subjected to peak acceleration values of approximately 0.2g during the earthquake. As a result of the shaking, the pile to pier connection failed at four of the piles near the end of the pier as shown in Fig. 3.14. In addition, two of the piles apparently rotated about 10º from their original vertical position as shown in Fig. 3.14. To provide lateral stability to the pier, three steel H-piles were driven as shown in Fig. 3.14 and 3.15 and lateral bracing put in place. In addition, the connections between the deck and the support piles was repaired.

Fig. 3.14 - Failure of the pile to deck connection at four piles near end of pier. (9.96779° N 84.74181° W).

Fig. 3.15 - Pier with additional support piles to stabilize the pier during repairs. (9.96812° N 84.74150° W).

4.0 Performance of Bridges

Because potentially liquefiable soil deposits in the western side of Costa Rica are primarily associated with alluvial deposits near rivers and streams, the GEER team inspected a number of bridges to look for liquefaction induced damage. Although liquefaction features were observed in a few cases, the team was unable to find any cases where liquefaction or lateral spreading caused any damage to bridge. Performance of bridge structures in Costa Rica was very good during this earthquake. Of the more than 4000 bridges in the country only two were damaged beyond repair. Most damage was associated with limited displacements as described in the subsequent sections on various bridges. Although bridge performance is not a "geotechnical aspect" of the earthquake per se, these sections are included in this report to document the observations which the team made as part of our inspection effort.

4.1 Rio Barranca Bridge

The Rio Barranca Bridge is located on Route 1 at latitude/longitude coordinates 9.9970 N 84.6946 W. It was constructed in 1944 as a joint effort between the Republic of Costa Rica and the United States of America. The bridge is approximately 110 meters in length spanning the Rio Barranca and is comprised of two sections: a bent-supported section on the east side of the bridge that is approximately 55 meters in length, and a simply-supported steel truss section on the west side of the bridge that is approximately 55 meters in length. A photo of the bridge taken during our site reconnaissance is shown in Fig. 4.1 and an aerial image of the bridge (courtesy of

Google Earth ™) is shown in Fig. 4.2. The bent-supported section of the bridge is comprised of five steel girders sitting on four reinforced concrete bents spanning the width of the bridge. The bent-supported section of the bridge may have had issues with scour in the past because it appeared the base of the bents had been encased in concrete with boulder-sized riprap. The steel truss portion of the bridge resembled the typical truss bridge commonly used throughout Costa Rica, particularly for railways. The west abutment of the steel truss portion of the bridge consisted of a large reinforced concrete abutment wall approximately 20 feet in height.

Fig. 4.1 - Photo taken of the Rio Barranca Bridge near the east abutment (9.99717° N 84.69409° W).

Fig. 4.2 - Aerial view of the Rio Barranca Bridge (courtesy of Google Earth ™). (9.9970° N 84.6946° W).

The Costa Rican Ministry of Transportation inspected the bridge just a few days after the September 5 event, and identified it as having sustained damage from the earthquake. The Ministry's investigation identified torsional buckling in a few members of the truss. Our investigation confirmed the torsional buckling in the truss (Fig. 4.3), though it is not immediately clear whether the earthquake caused the distress. Rust spots were visible in distressed areas due to the torsional buckling, suggesting that the damage may have occurred prior to the September 5 earthquake. In addition to the buckling, our inspection of the bent-supported section of the bridge showed that the connection plates and fasteners between the bridge and the bent on the southern part of the bridge appeared to have been pulled out of the concrete approximately 25-50 mm (1-2 inches), as shown in Fig. 4.4.. Two water pipelines approximately 0.5 m (20 inches) in diameter were observed to run parallel to the bridge deck on both sides of the bridge. Inspection of the pipeline on the south side of the bridge identified what appeared to be possible of evidence of compression of the pipe due to a slightly crooked alignment (Fig. 4.5). However, no evidence of compression in the bridge deck was apparent. The pipeline on the north side of the bridge did not show the same crooked alignment as the southern pipeline; however, significant leakage was observed at one of the collared joints near the west abutment of the bridge.

Fig. 4.3 - Torsional buckling in certain members of the truss bridge (9.99704° N 84.69480° W).

Fig.4.4 - Pull-out of the connections between the deck and the bent on the southern half of the bridge (9.99706° N 84.69436° W).

Fig. 4.5 - Crooked water pipe adjacent to the south side of the bridge (9.99705° N 84.69412° W).

The GEER reconnaissance team identified possible evidence of liquefaction along the east bank of the river immediately south of the bridge. Remnants of what appeared to be subsided sand boil approximately 1.5 meters (5 feet) in diameter were visible, along with traces of what appeared to be residual runoff sand that had flowed towards the river Fig. 4.6 and 4.7). However, we could find no strong visible evidence that liquefaction had caused damage to the Rio Barranca Bridge.

Fig. 4.6 - Evidence of a subsided sand boil due to liquefaction (9.99688° N 84.69438° W).

Fig. 4.7 - Ejecta and sand runoff adjacent to the subsided sand boil (9.99676° N 84.69442° W).

4.2 Rio Poas Bridge

The Rio Poas Bridge is located on Route 1 at latitude/longitude coordinates 10.0021 N 84.3107 W. According to a placard on the east side of the bridge, the bridge was constructed in 1970. The bridge is approximately 130 meters in length spanning the Rio Poas and appears to have a slight horizontal curve. An aerial view of the bridge (courtesy of Google Earth ™) is shown in Fig. 4.8, and a photo of the bridge taken during our reconnaissance is shown in Fig. 4.9. The bridge consists of large reinforced concrete girders, although exact measurements could not be obtained due to the presence of wasps beneath the bridge. The bridge is supported by two large, square reinforced concrete columns that are an estimated 24-30 meters (80-100 feet) in length. The bridge includes a steel guardrail on both sides, though many sections of the guardrail were either damaged or missing at the time of our reconnaissance. This damage to the guardrail likely occurred before the September 5 earthquake.

Fig. 4.8 - Aerial image of the Poas River Bridge (courtesy of Google Earth ™). (10.0021° N 84.3107° W).

Fig. 4.9 - Photo taken of the Poas River Bridge adjacent to the east abutment (10.00238° N 84.31026° W

The Costa Rican Ministry of Transportation inspected the bridge just a few days after the September 5 event, and identified it as having sustained damage from the earthquake. While our reconnaissance team confirmed this report, the damage we observed appeared relatively minor. Investigation of the bridge deck at the abutments revealed an offset of 76 mm (3 inch) at the west abutment (Figs. 4.10 and 4.11) and an offset of 25 mm (1 inch) at the east abutment (Fig. 4.12). According to the Costa Rican Ministry of Transportation, the bridge deck was designed to have offsets of approximately 25-50 mm (1-2 inches) at the abutments. In addition, vertical offsets of

about 25 mm (1 inch) were measured at the east abutment (Fig. 4.13). These offsets suggest that the entire bridge permanently displaced about 25 mm (1 inch) to the east and settled about 25 mm (1 inch). Inspection of the guardrail near the west abutment showed damage to the concrete and exposed rebar (Fig. 4.14), possibly due to pounding between the bridge and the abutment during the earthquake.

Fig. 4.10 - Longitudinal offset at the west abutment (10.00188° N 84.31129° W).

Fig. 4.11 - Longitudinal offset of about 76 mm (3 inches) at the west abutment.

Fig. 4.12 - Longitudinal offset of about 25 mm (1 inch) at the east abutment (10.00231° N 84.31025° W).

Fig. 4.13 - Vertical offset of about 25 mm (1 inch) at the east abutment.

Fig. 4.14 - Possible evidence of pounding beneath the guardrail at the west abutment (10.00193° N 84.31131° W).

4.3 Rio Tempisque Bridge

The bridge over the Rio Tempisque, also known as La Amistad Bridge, is located on Route 18 at latitude/longitude coordinates 10.2468 N 85.2468 W. The bridge is approximately 780 meters long, 15 meters wide, and consists of two sections: a cable-stayed section to the west that is approximately 260 meters long, and a box-girder section to the east that is approximately 520 meters long. A 3-dimensional depiction of the bridge (courtesy of Google Earth ™) is shown in Fig. 4.15. A photo taken of the bridge during the site reconnaissance is shown in Fig. 4.16.

Fig. 4.15 - 3-dimensional representation of the bridge over the Rio Tempisque (courtesy of Google Earth ™) (10.2468° N 85.2468° W).

Fig. 4.16 - Photo of the bridge over the Rio Tempisque taken during our reconnaissance from near the west abutment (10.24555° N 85.24895° W).

The bridge was completed in 2003 and was designed and constructed as a joint effort between Costa Rica and Taiwan. According to a commemorative plaque near the west abutment, the cable-stayed portion of the bridge is asymmetric with the west side spanning 90 meters and the east side spanning 170 meters. A total of 18 steel cables support the suspension bridge. The H-pylon for the suspension bridge is 79.55 meters high and supports 9 pairs of cables. The pylon consists of two large columns, each supported by 12 drilled shafts that are each 1.5 meters in diameter and 23 meters in length. The total estimated weight supported by the cables is approximately 4,000 tons. The box-girder section of the bridge is supported by a total of eight single-column reinforced concrete bents. Each bent is founded on 12 drilled shafts that are each 1.5 meters in diameter and 23 meters in length.

The Costa Rican Ministry of Transportation inspected the bridge just a few days after the September 5 event, and identified it as having sustained damage from the earthquake. Reported damage was generally limited to concrete spalling at the joint between the cable-stayed bridge and the box girder bridge due to pounding (Fig. 4.17). Our investigation confirmed that spalling in the concrete had occurred at the joint between the two bridges (Fig. 4.18), resulting in the exposure of steel rebar in a few locations. We measured a gap of approximately 25 mm (1 inch) at the joint between the two bridge sections (Fig. 4.19). Investigation of the east abutment of the bridge revealed a large crack about 25 mm (1 inch) in width spanning the width of the abutment slab, as shown in Fig. 4.20. This crack appeared to have been caused by differential settlement or slope movement beneath the slab. It is unclear whether these settlements or movements occurred as a result of the September 5 earthquake or prior to it. Visual inspection of the bents from the east abutment showed no evidence of tilting or other damage. No evidence of liquefaction was observed in the vicinity of the bridge abutments.

Fig. 4.17 - Spalled concrete and exposed rebar due to pounding between the cable-stayed bridge and the box girder bridge (courtesy of the Costa Rica Ministry of Transportation) (10.24678° N 85.24685° W).

Fig. 4.18 - Evidence of pounding observed by the reconnaissance team at the joint between the box girder section and the cable-stayed section of the bridge (10.24678° N 85.24685° W).

Fig. 4.19 - Gap of approximately 25 mm (1 inch) between the box girder and cable-stayed sections (10.24670° N 85.24682° W).

Fig. 4.20 - Transverse crack observed across the abutment slab at the east abutment (10.24889° N 85.24262° W).

4.4 Rafael Iglesias Bridge

The Rafael Iglesias bridge spans over the Colorado River, approximately 3 km west of Poás bridge. This inverted concrete arch structure was designed by renowned structural engineer T.Y. Lin and placed in service in 1974. The bridge deck lies on top of an inverted arch structure supported by two pivots held in place by longitudinal cables inside segmented panels constituting the arch. Tension in the bottom chord of the truss is carried by steel cable bundles which are sheathed and run continuously on both sides of the structure to anchor blocks cast on opposing bridge abutments.

Overall the bridge performance following the Nicoya earthquake was good, with no noticeable cracking or excessive separation between bridge segments. However, the Costa Rican Ministry of Transportation inspected the bridge a few days after the earthquake and identified some potential problems owing to the offset between the bridge and the abutment. The GEER team observed that the gap between the bridge and the southeast abutment had increased by about 1.5 inches from its original position as shown in Fig. 4.25 (a) and (b). This offset had caused the metal sheathing around two of the cables to be pulled apart so that the steel wire cables were exposed to the atmosphere. Although this does not pose any immediate threat to the safety of the bridge, the potential for accelerated corrosion is significantly increased. In addition, the movement of the bridge in the northwest direction has reduced the seat length on the abutment to only about 7 inches (see Fig. 4.25(c)).

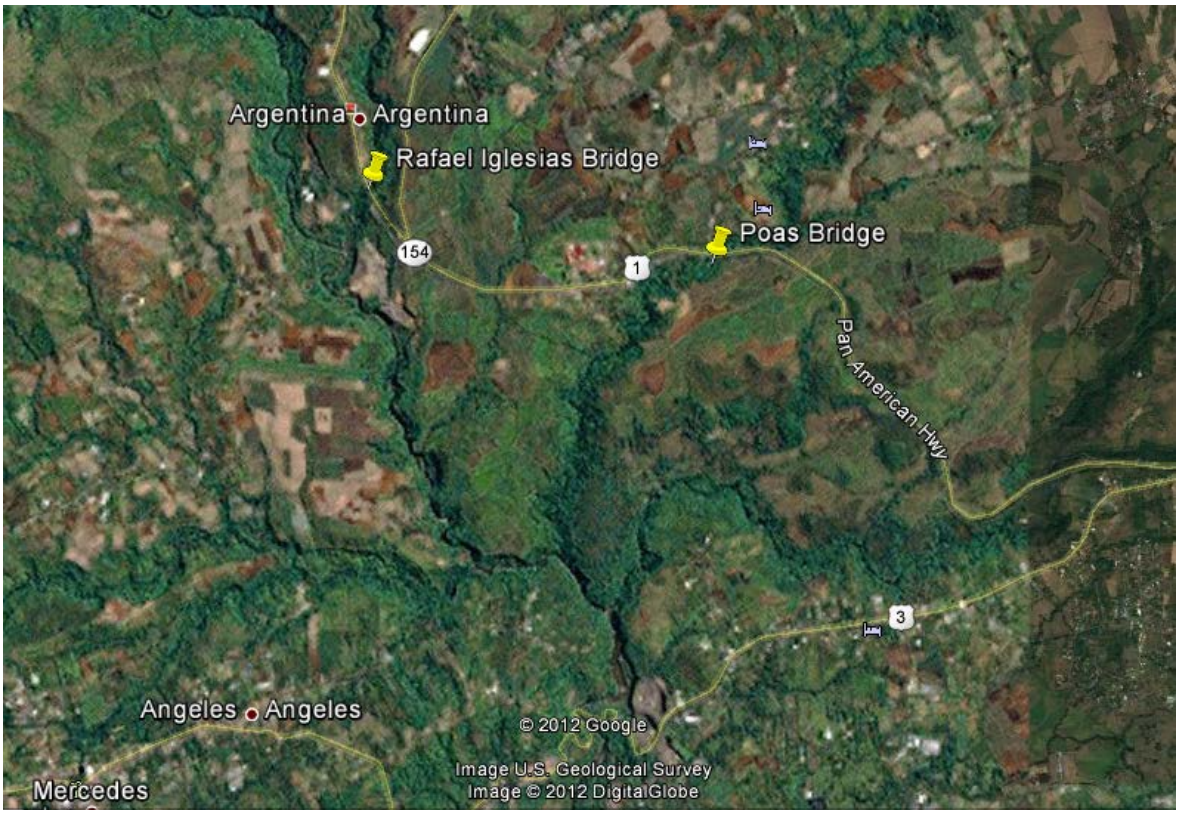

Fig. 4.21 - Rafael Iglesias bridge over the Colorado river (Courtesy Google Earth ™) (10.0222° N 85.3587° W).

Fig. 4.22 - Pivot and inverted arch, Rafael Iglesias bridge (10.01907° N 84.35651° W).

Fig. 4.23 - Inverted arch section of Rafael Iglesias bridge

Fig. 4.24 - View of segmented inverted arch section, Rafael Iglesias bridge

Fig. 4.25 Offset of bridge relative to abutment at Iglesias bridge of about 1.5 inches. The offset ruptured the metallic sheath surround the tension cable exposing them to increased corrosion and reduced the seat distance for the abutment. (10.02801° N 84.36015° W)

4.5 Sarapiqui-LaVirgen Bridge

This single span steel truss bridge on high 126 with a span length of approximately 71 m crossed the Sarapiqui River as shown in Fig. 4.26. This bridge is located about 170 km for the fault rupture Fortuitously, a strong motion recording station (HVRG) was located within about 250 m of the bridge and the peak ground acceleration was only 0.05 g. A photograph of the bridge prior to the earthquake is provided in Fig. 4.27.

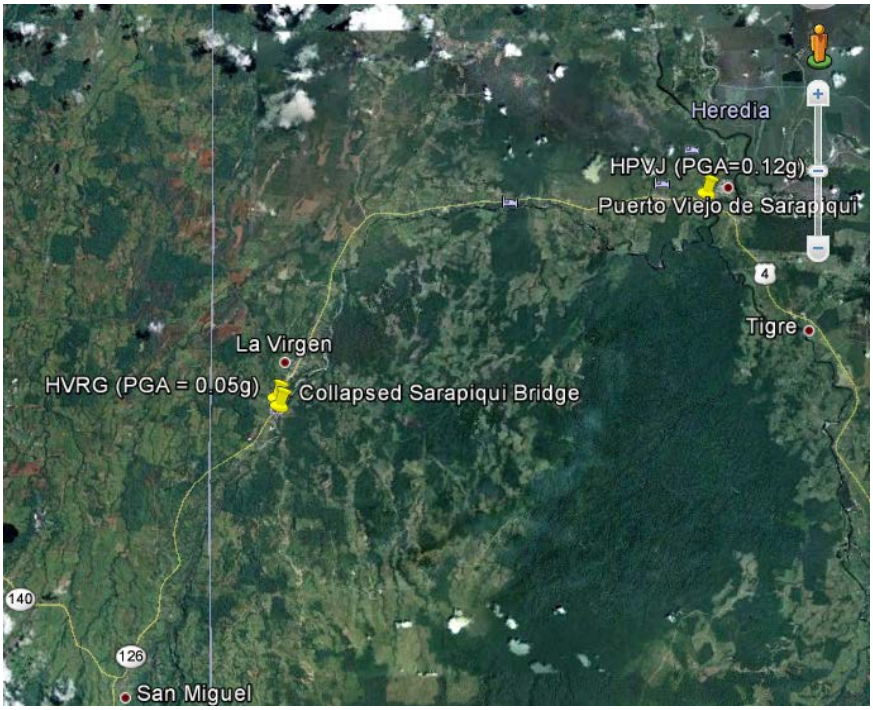

Fig. 4.26 Location of collapsed Sarapiqui bridge relative to strong motions recording stations

Fig. 4.27 - Bridge De Hierro Sobre El Rio Sarapiqui-La Virgen (10.38825° N 84.13859° W).

Photographs looking along the longitudinal axis of the bridge from one abutment (a) before and (b) after the earthquake are shown in Fig.4.28. The bridge appears to be a 1930s vintage bridge with built-up sections to form the truss members. The bridge had been demolished prior to the arrival of the GEER team and new pile foundations were being driven to support a replacement bridge. Given that the bridge was relatively old and the ground motions were quite low, it seems likely that the bridge failed by falling off the support on one side which led to a failure of the top truss. A similar failure occurred to a steel girder bridge at Rio Estella during the 1991 Limon Cost Rica earthquake. A newer, well constructed bridge would have survived this low acceleration level with little problem.

Fig. 4.28 – Photographs in the longitudinal direction of the De Hierro Sobre bridge over the Sarapiqui river (a) before and (b) after the earthquake. The bridge collapsed into the river during the earthquake despite relatively low acceleration level. (photos courtesy of Yamil Herrera) (10.39000° N 84.13736° W)

4.6 Nosara Bridge

In contrast to the poor performance of the truss bridge over the Sarapiqui river, this two span bridge at Nosara (≈70 m length) shown in Fig. 4.29 weathered the earthquake with no apparent damage with the exception of some sloughing of the steeply inclined approach fill. The abutments and center pier, shown in Fig. 4.29, were supported by a framework consisting of eight steel H piles (HP12x63) driven 8 m into the underlying soil profile. The bridge was attached with a pin connection to a plate section which was welded atop the eight H piles as shown in Fig. 4.30. A recording station in Nosara about 2 km from the bridge recorded a peak acceleration of 1.38 g. This case history points to the fact that well-constructed bridge can perform very well despite strong ground shaking, particularly if the bridge support seats are adequate.

Fig. 4.29 Single span steel bridge in Nosara which performed without damage despite peak ground accelerations of 1.38g in the vicinity owing to the proximity to the fault rupture. Pile foundations at the abutment were in the same configuration as for this central pier.

Fig. 4.30 Pin connection between bridge and pile supported abutment consisting of eight H piles.

5.0 Ground Response Observations

5.1 Ground Response/Soil Amplification

5.1.1 Fraijanes Agricultural Station (AFRA station)

Several engineers and seismologists made reference to the fact that soil amplification was noticed in the volcanic soil deposits near the region of the Volcán Poás. The closest station that represents this region is the Fraijanes experimental agricultural station, where an accelerometer was installed by LIS-UCR and labeled AFRA station. The instrument is a Refraction Technologies, Inc. (REFTEK) accelerometer placed directly on the concrete slab of the single story building as shown in Figure WW-1. This accelerometer is connected to the Internet and is online recording continuously the three components of acceleration.

Given that the peak ground accelerations at the AFRA station were higher than some neighboring stations in more firm rock. The decision was made to conduct a geophysical survey with the MASW equipment to obtain a profile of shear wave velocity of these volcanic soils. The survey was performed in an open grassy lot directly adjacent to the northeast side of the administration building and minimal to no external noise was present during testing. Data referencing existing characterization of the subsurface soils and rock was not available for any of the three survey locations. The site manager, Sr. Joaquin Secaira Navarrete, of the agricultural research station at Fraijanes station was familiar with the soils at the site and his description of the subsurface is listed in Table WW-1.

Table 1.1 Verbal description of site soils at Fraijanes Station

Thickness	Description
~ 50 – 60 cm	top soil, black
~ 25 – 30 cm	yellowish silty clay
~ 100 cm	black soil; mixture of black, volcanic sand and yellow conglomerate
~ 39 m	volcanic sand - - layers of different colors
> 40 m	Rock / lava cooled /

5.1.1.1 MASW Surveys

Active measurements were obtained by installing (24) spike-coupled, vertically-based 14 Hz geophones to a multichannel signal recorder (SeisTronix RAS-24). While traditionally MASW surveys are performed with lower frequency 4.5 Hz geophones, Park (2006) stated that the effectiveness of 10 – 20 Hz geophones is often comparable to that of the low-frequency geophones. A 20lb sledgehammer and an aluminum plate (20 x 20 x 2.5 cm) were used as the

active seismic source. The surveys included the stacking of 7 blows to the strike plate to reduce any background noise and improve the signal to noise ratio. A reverse strike was then conducted to capture the signal from the other direction. The source was offset 5 meters from the first geophone and the spacing between geophones was 1 meter, resulting in a total linear array of 28 meters for each survey. The sampling frequency was 0.5 ms and the total recording length was 2 seconds. Two separate orthogonal surveys were performed at the Fraijanes station.

5.1.1.2 Data Analysis

Data processing was performed using SurfSeis 3.0 (Kansas Geologic Survey 2010). The program interprets and extracts Rayleigh surface waves from a field record, converts the time-velocity data to the frequency domain for frequency analysis, generates a dispersion curve, and finally a one-dimensional velocity profile is developed from the inversion of the dispersion curve.

First, the raw seismic data in SEG-2 format was converted into the KGS format utilized by the program. Once each file was suitably formatted, a dispersion analysis was performed on each record. The dispersion analysis essentially converts the time-acceleration data recorded in the field to the frequency domain. A dispersion curve, also called an overtone image, was developed for each data file which was essentially a dispersion curve representing the relationship between phase frequency, phase velocity, and amplitude. The dispersion curves were calculated using a frequency range from 3 to 50 Hz and a phase velocity range between 10 and 1000 m/s. The fundamental mode was manually identified for each dispersion curve. Finally, an inversion process was completed once the fundamental mode was identified from each dispersion curve. The inversion process resulted in a 1D velocity profile for each linear array.

5.1.1.3 Shear Wave Profiles

Both the dispersion curves and the 1D shear wave velocity profiles for each survey location were critically evaluated considering all the data obtained in the field. Various interpretations of the dispersion curves were considered. Ultimately the 1D profiles that best represented the existing knowledge of the site were selected and presented below in the corresponding figures for each of the sites investigated.

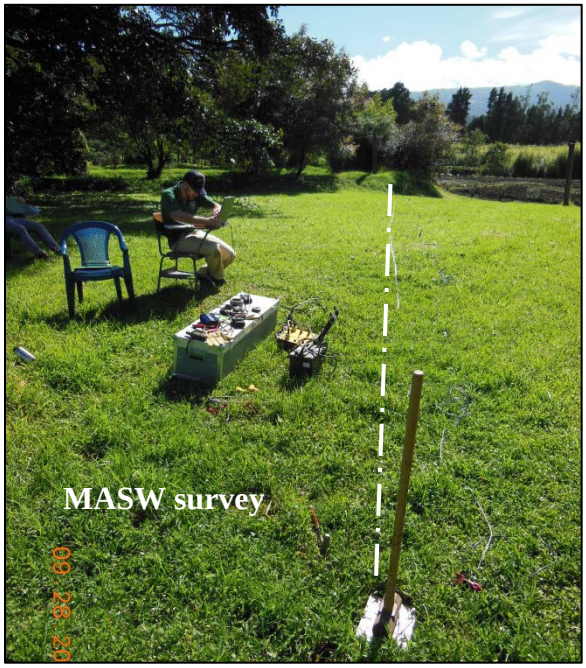

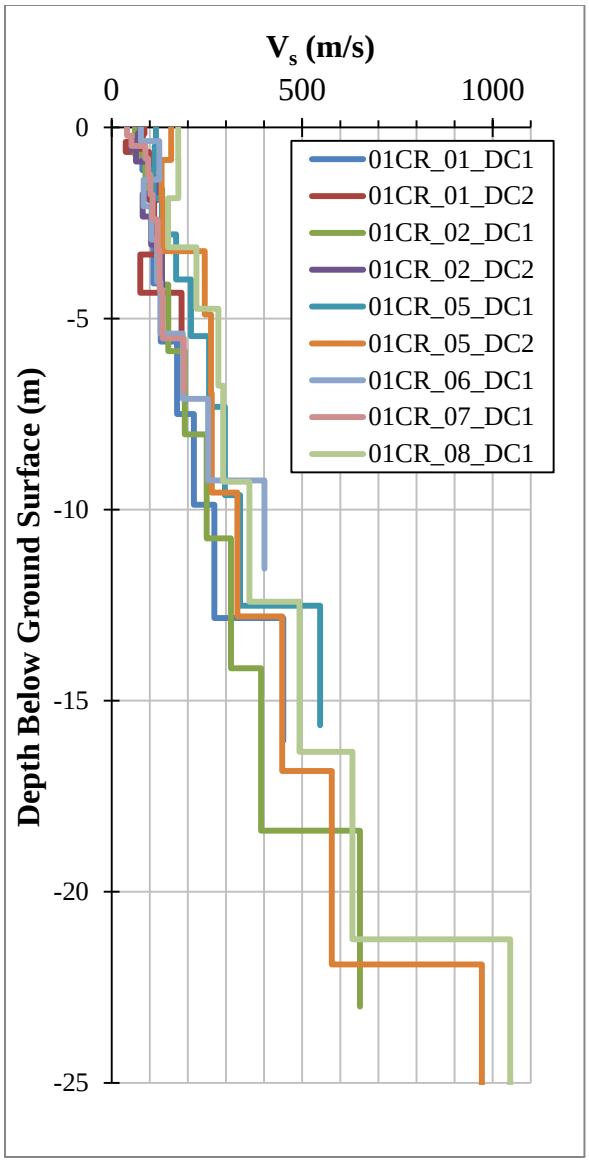

Fig. 5.1 – MASW Shear Wave Velocity (V_s) Profile near the Fraijanes Station (AFRA), which was reported to undergo amplification in volcanic soils. (10.13747° N 84.19305° W).

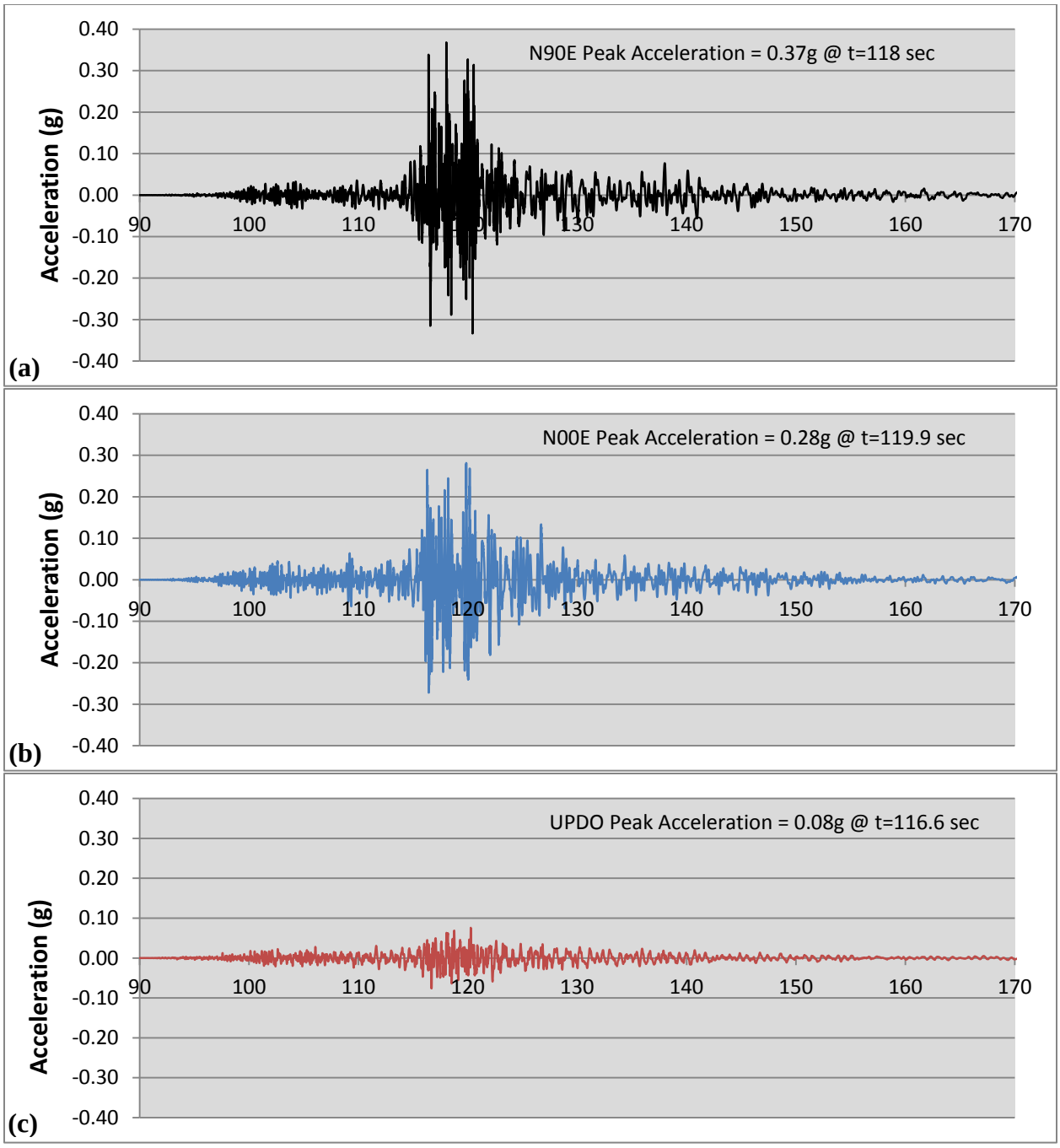

Fig. 5.2 – Acceleration time history for the AFRA station, Fraijanes, Alajuela Province. (a) Horizontal N90E, (b) Horizontal N00E, and (c) Vertical UPDO

5.2 Nosara Station, Nosara, Guanacaste

The Nosara area is located in the Nicoya Peninsula near the Pacific Coast, slightly northwest of the town of Samara. This location had very little damage, almost none was observed, but it was strongly felt by the residents. This was the location visited by the team that was the closest to the epicenter. An accelerometer is located inside a single story Biblioteca (Library) David Kitson.

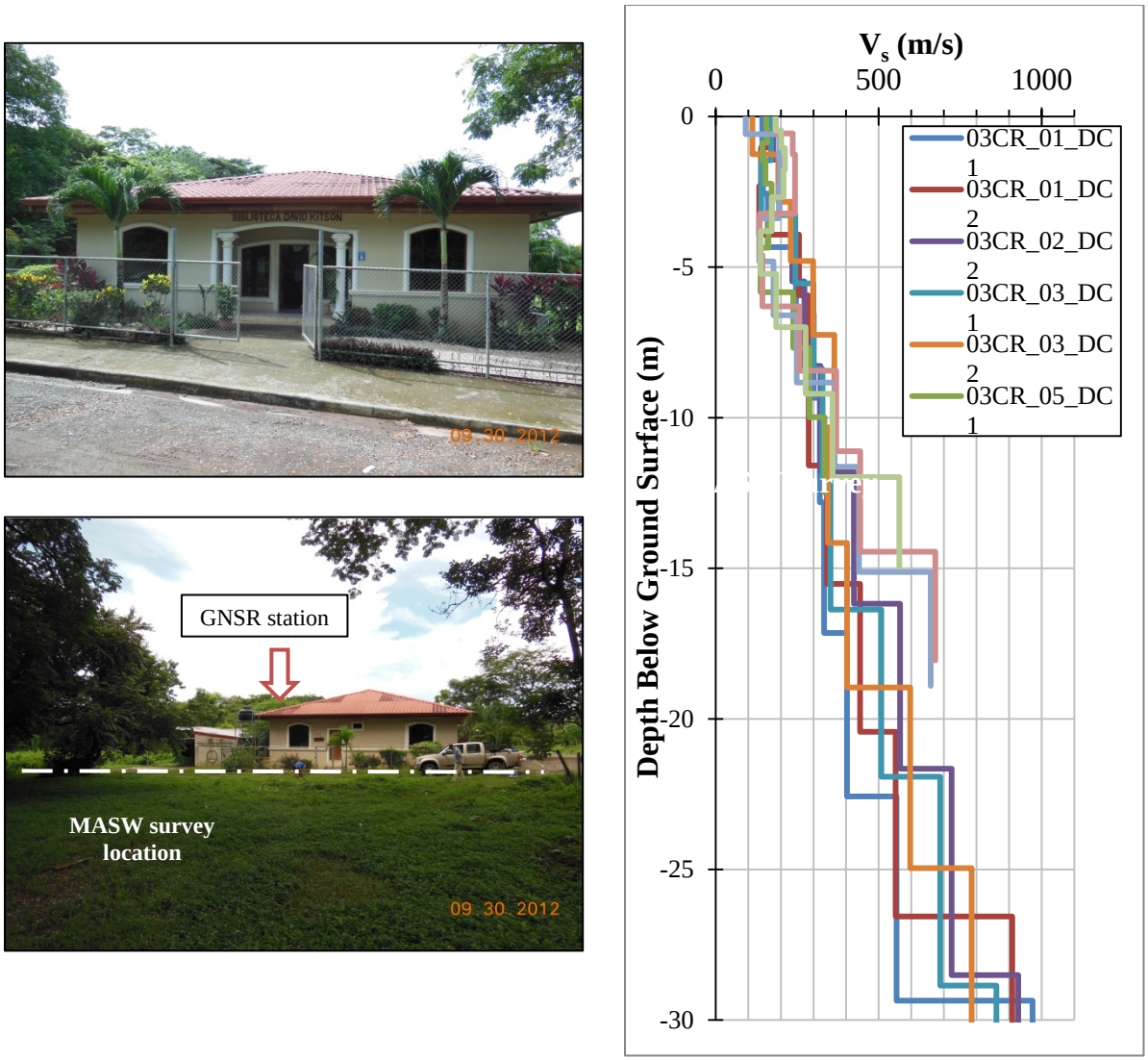

Fig. 5.3 – MASW Shear Wave Velocity (V_s) Profile in the Biblioteca David Kitson in Nosara (GNSR), reported one of the largest amplitudes in the vertical direction. (9.97902° N 85.648

5.3 Geotechnical Local Site Effects in the Provincia de Alajuel

The geotechnical conditions from the Poás volcano highlands to the foothills of these volcanic soils consist of rugged and highly vegetated terrain. Several geotechnical failures due to topographic effects along ridges and slope instabilities were observed. It is also believed that the ground conditions are prone to ground motion amplification from an input bedrock ground motion. The ground conditions coupled with poor drainage and mediocre construction practices precipitated damage and occasional collapse of structures. Often when ground displacement was pronounced structures were detached from each other as they started moving as monoliths over soft moving ground. Liquefaction was not observed, but slopes and walls with poor drainage were prime candidates to experience damage.

Fig. 5.4 – Construction near steep slopes: retaining walls and slope failure (a) Leaning retaining wall and large deformations caused evacuations; (b) Large crack openings parallel to the alignment of wall, (c) detached stairwell of structure built near a slope, minor reinforement.

Fig. 5.5 – Structures became inhabitable. (a) Rear access porch became detached from structure, no apparent structural tie of porch to structure; (b) The shear displacement near retaining wall caused masonry construction to collapse in back patio of lower house.

Fig. 5.6 – Cemetery damage in the town of Grecia (a) Excessive tilting, subsidence, and bearing capacity failures; likely due to construction over old underground burial sites; (b) Perimeter gravity retaining wall failed at different locations.

Fig. 5.7 – Slope failures near built dwellings and roads. (a) Collapse of steep bank on to small house; (b) Light construction single story and carports built on top of steep slope with water utilities located a toe of slope, likely contributed to the slope failure.

6.0 Performance of Dams

The Costarican Institute of Electricity (Instituto Costarricense de Electricidad, ICE) has a network of accelerometers on the most important dam structures in the country. The GEER team met with ICE to evaluate the performance of dam in the affected earthquake region. The data collected by the ICE was for the main event of September 5th and two aftershocks. The epicenters of the events were determined by the "Red Sismologica Nacional (RSN), which uses data from ICE and UCR. The location of the instrumentation network and the location of the epicenters are shown in Figure 6-1.

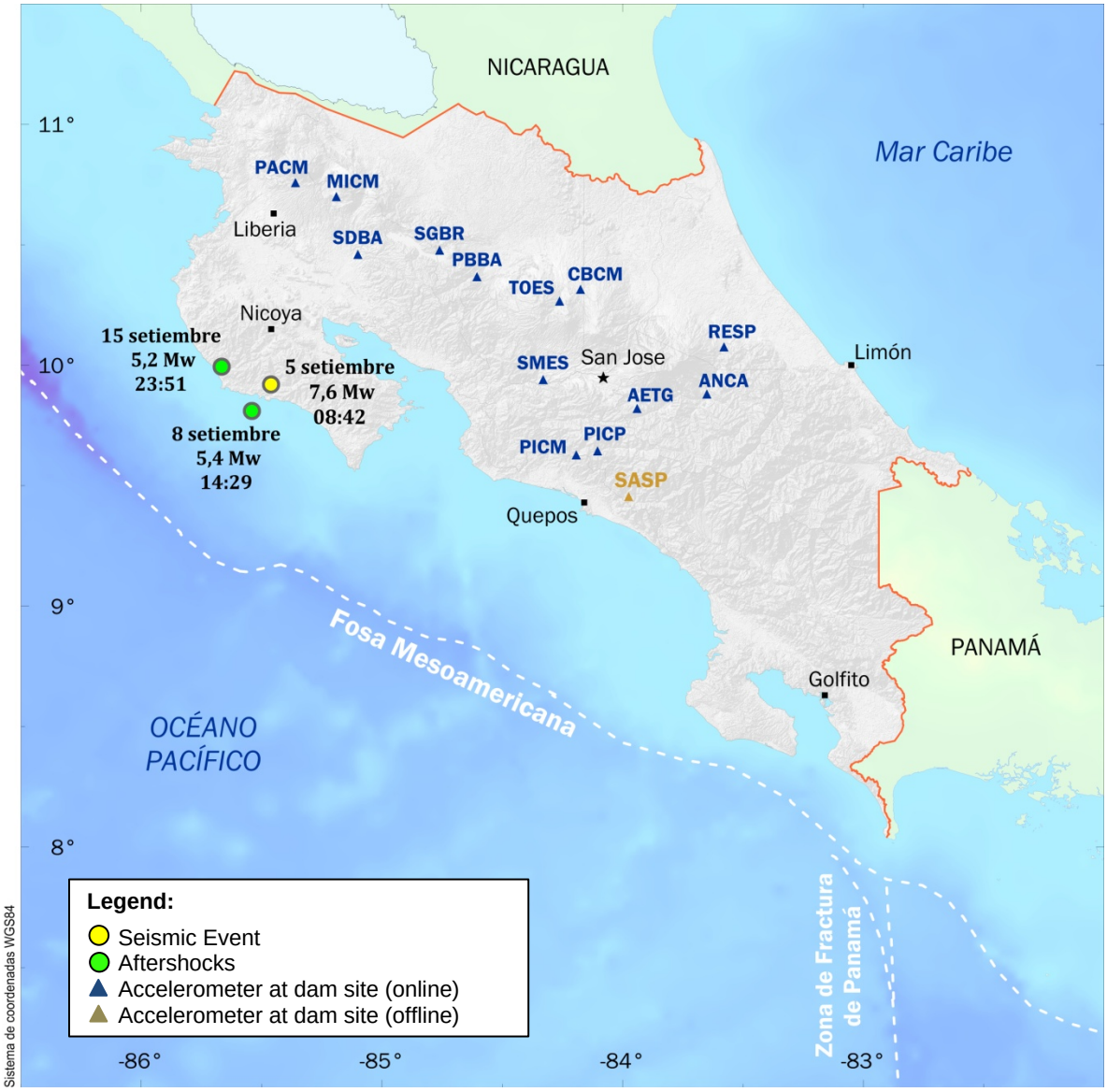

Fig 6.1 - Location of ICE dams and epicenters for main event and aftershocks.

In addition to the locations shown in the figure above the peak accelerations recorded at these structures (mainly earth dams) for power production are shown in Table 6.1. In this table each component (1 vertical and 2 horizontal) of the peak ground accelerations recorded are presented.

The accelerometers are installed with each horizontal component aligned in the longitudinal and transverse direction of the dam. The records shown are for the dam projects that recorded data only, those that were malfunctioning, corrupt, or truncated were eliminated from the table.

Table 6.1 Peak ground accelerations recorded by ICE during the Sept. 5, 2012 Earthquake

Dam Project Name	Station	Code	Coordinates		Epicentral Distance (km)	PGA (cm/s^2)		
			Latitude	Longitud		Vertical	Horiz-1	Horiz-2
Sandillal	SDCR	9E60	10,461	-85,100	72,193	255.00	223.00	390.00
	SDMT	A078				99.70	139.20	136.50
	SDBA	9E5F				No record due to power problems at site		
Sangregado	SGCR	A079	10,477	-84,760	99,384	31.44	67.88	92.08
	SGBR					33.28	56.70	60.41
	SGBA					27.22	52.99	92.31
Miravalles	MICM	AB3E	10,701	-85,193	116,439	36.22	63.08	37.02
Toro II	TOCR	9F88	10,266	-84,260	138,733	15.96	30.00	32.93
	TOES	9F89				15.34	20.32	23.44
Angostura	ANCA	91AC	9,871	-83,642	201,982	30.85	73.27	51.99
	ANCR	91AB	9,880	-83,650	201,070	Loss of connectivity		
Peñas Blancas	PBCR	2092	10,368	-84,605	107,242	31.79	30.59	67.05
	PBBA	2295				23.29	27.23	56.82
Cariblanco	CBCM	3760	10,315	-84,175	149,328	Corrupt record		
	CBTO	2860	10,304	-84,188	147,560	25.62	87.84	79.07
San Miguel	SMCR	2091	9,940	-84,330	125,561	-	-	-
	SMES	2296				11.11	20.73	23.36

Notes: The station codes include the location of the accelerometer "CR" = crest; "MT" = mid slope downstream; "BA" = base of dam; and "ES" = abutment.

In general, the dam sites recorded accelerations less that 100 cm/sec^2 or 0.10g, with the exception of the Sandillal Project, which recorded accelerations from 0.22g to 0.40g. The Sandillal project warrants further discussion in the following section of this report. All dam sites experienced low levels of damage consisting of deformations and cracks that did not impact the power production operations. It can be concluded that the level of engineering that went into the design and construction of these dams resulted in good performance.

6.1 Dam El Sandillal Earthquake Record

This dam site was the closest one to the epicenter, located only 72.2 km. The locations of the accelerometers are shown in the aerial photograph in Figure 6.2. This dam is an earthen dam with a clay core and rockfill revetment completed in 1992. The maximum horizontal acceleration of 0.40g was recorded along the transverse direction at the crest of the dam. In the longitudinal direction along the crest, the horizontal acceleration was recorded at 0.22g and the vertical acceleration was recorded at 0.26g. The anticipated amplification was noted by the other record available at the mid slope of the dam, which indicated a near double in magnitude. Unfortunately the record at the base of the dam was not available due to power issues during the earthquake

event. However, the LIS-UCR network of accelerometers recorded in nearby free-field stations ranged from 0.134g (Ingenio Taboga, Cañas) to 147g (Biblioteca Cañas) at sites.

Fig. 6.2 - Aerial photograph of Sandillal dam showing the accelerometer locations in red. (10.46173° N 85.09958° W).

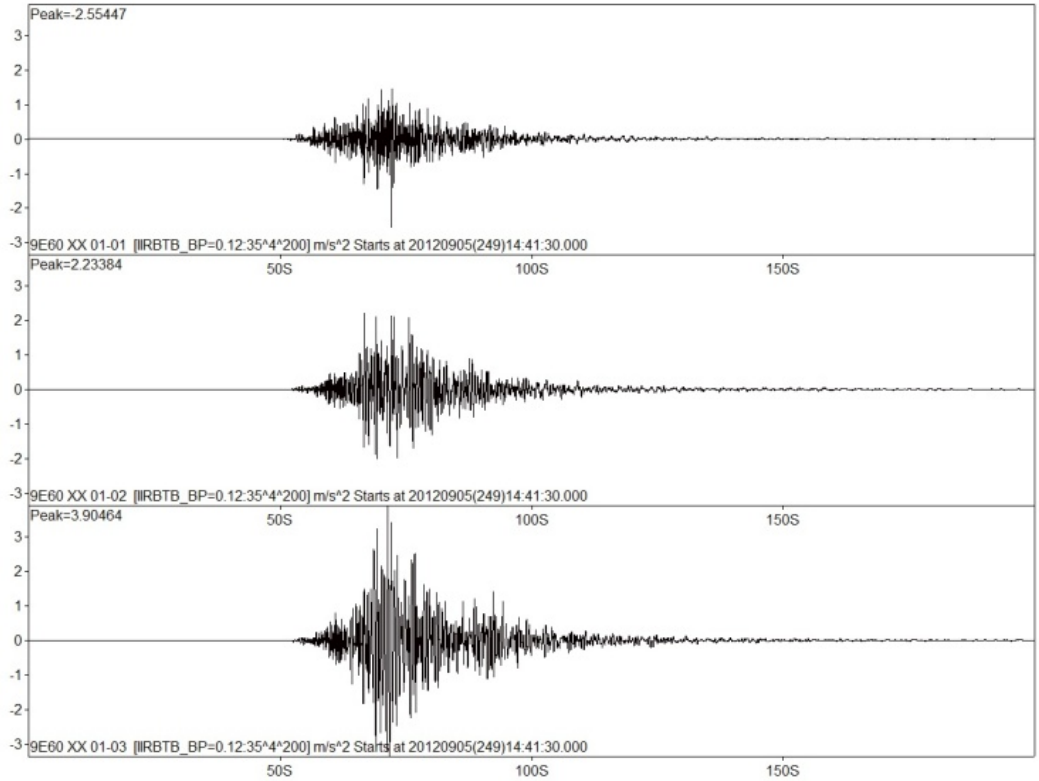

Fig. 6.3 - Acceleration time history for the three coponents at the crest of Sandillal Dam, September 5, 2012 main event (Vertical, Horiz-1, and Horiz-2).

The level of ground shaking at the crest (0.40g) is considered severe with the potential of generating moderate damage. Based on site visits by the ICE personnel the reported damage consists of small longitudinal cracks along the crest and a maximum settlement of about 12cm.

References

Alvarez, C. (2012). “Pochote Reconstruction after Earthquake Costa Rica” http://www.betterplace.org/en/projects/10789-pochote-reconstruction-after-earthquake-costa-rica

Cotza Rica (2012) “Earthquake of 7.6° in Nicoya caused only moderate damage” http://www.coztarica.com/2012/09/06/earthquake-of-7-6-%C2%B0-in-nicoya-caused-only-moderate-damage/

Dutch. S (2012) Geology of Cost Rica, Natural and Applied Sciences, Univ. of Wisconsisn-Green Bay https://www.uwgb.edu/dutchs/CostaRica2008/CRGeology.HTM

Edodes (2012). Playa Tivives, Costa Rica Septemeber 5, 2012, http://edodes.tumblr.com/post/30976488839/costa-rica-playa-tivives-september-05-2012

LIS (2012a) “Maps related to the Sept. 9, 2012 Samara, Costa Rica Earthquake.” http://www.lis.ucr.ac.cr/mapas/2012-09-05-10:20:21

LIS (2012b) Contours of Intensity for September 9, 2012 Samara, Costa Rica, Earthquake.” http://www.facebook.com/lis.ucr.ac.cr?ref=ts&fref=ts

LIS (2012c) “Animation of the rupture of the earthquake of Samara”, http://www.lis.ucr.ac.cr/mapas/2012-09-05-10:20:21/samara3.gif,

LIS (2012d) “Process of rupture of the Samara earthquake” http://www.lis.ucr.ac.cr/pdf/samara_2/

Reuters (2012) “Magnitude 5.6 quake hits Costa Rica, Sept 8, 2012, Photo by Juan Carlos Ulate http://news.yahoo.com/photos/earthquake-rocks-washington-area-1314124172-slideshow/man-walks-past-cracks-beach-caused-earthquake-nosara-photo-190442923.html

United States Geological Survey (2012) "Magnitude 7.6 - COSTA RICA: Summary".. http://comcat.cr.usgs.gov/earthquakes/eventpage/usc000cfsd#summary

Youd, T.L., Rollins, K.M., Salazar, A.F., and Wallace, R.M. (1992) “Bridge Damage Caused by Liquefaction During the 22 April 1991 Costa Rica Earthquake.” Procs. 10th World Conference on Earthquake Engineering, Madrid, Spain, 19-25 July 1992, Vol. 1, pp. 153-158